Distinct Plasmonic Manifestation on Gold Nanorods Induced by the Spatial Perturbation of Small Gold Nanospheres

ARTICLE *in* NANO LETTERS · JANUARY 2012

Impact Factor: 13.59 · DOI: 10.1021/nl2041063 · Source: PubMed

6 AUTHORS, INCLUDING:

Lei Shao
Chalmers University of Technology
28 PUBLICATIONS **926** CITATIONS

SEE PROFILE

NANO LETTERS

Letter

pubs.acs.org/NanoLett

Distinct Plasmonic Manifestation on Gold Nanorods Induced by the Spatial Perturbation of Small Gold Nanospheres

Lei Shao,[†,§] Caihong Fang,[†,§] Huanjun Chen,[†] Yat Cho Man,[†] Jianfang Wang,*[,†] and Hai-Qing Lin[†,‡]

[†]Department of Physics, The Chinese University of Hong Kong, Shatin, Hong Kong SAR, China

[‡]Beijing Computational Science Research Center, Beijing 100084, China

Supporting Information

ABSTRACT: The plasmon coupling between a Au nanorod and a small Au nanosphere has been studied with scattering measurements, electrodynamic simulations, and model analysis. The spatial perturbation of the nanosphere leads to distinct spectral changes of the heterodimer. The plasmonic responses, including Fano resonance, are remarkably sensitive to the nanosphere position on the nanorod, the gap distance, and the nanocrystal dimensions. The nanosphere dipole is intriguingly found to rotate around the nanorod dipole to achieve favorable attractive interaction for the bonding dipole−dipole mode. The sensitive spectral response of the heterodimer to the spatial perturbation of the nanosphere offers an approach to designing plasmon rulers of two spatial coordinates for sensing and high-resolution measurements of distance changes.

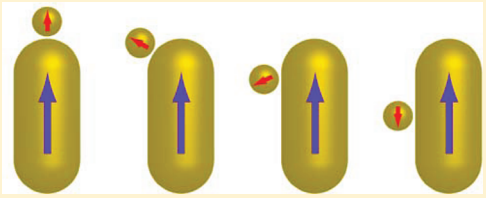

KEYWORDS: *Assembly, Fano resonance, gold nanorods, gold nanospheres, heterodimers, plasmon coupling*

The rich optical properties of noble metal nanocrystals stem from the localized surface plasmon resonances that can be excited by electromagnetic waves. When metal nanocrystals are placed in close proximities, their plasmon resonances can couple together, leading to spatial electromagnetic energy redistributions and wealthy changes in the light-scattering and absorption spectra.[1] Furthermore, near-field interactions enable the excitation of new plasmon modes, such as high-order electric multipole and magnetic dipole plasmon modes.[2] The interferences between different plasmon modes thereafter result in several fascinating phenomena in coupled metal nanostructures, such as spectral splitting,[3] plasmonic Fano resonance,[4] and electromagnetically induced transparency.[5]

Extensive investigations have been made on understanding[1,6] and modulating[7−9] the plasmon coupling between metal nanocrystals due to its potentials in various applications. For example, coupled metal nanostructures can serve as one- and three-dimensional plasmon rulers[10,11] owing to the strong dependence of the scattering spectrum on the interparticle spacing as well as the spatial configuration. The plasmon coupling-induced spectral changes and Fano resonances have been employed for developing biological and chemical sensors with greatly improved sensitivities,[1,12−14] optical switches,[15] and metamaterials and novel optical media.[4,5] Additionally, the dramatic enhancement of the electric field at the gap region arising from the electromagnetic energy redistribution brought by plasmon coupling has been widely utilized for plasmon-assisted polymerization,[16] high-harmonic amplification,[17] nanometric optical tweezers,[18] and various types of plasmon-enhanced spectroscopies.[19−21]

A majority of previous fundamental studies of plasmon coupling have focused on the interactions between the plasmons carried by two identical metal nanocrystals in a homodimer. Only dipole−dipole bonding plasmon modes are usually active for homodimers under light excitation due to their symmetry in both shape and material.[22−24] Heterodimers of metal nanocrystals exhibit richer plasmon coupling behaviors arising from the symmetry breaking. A few recent studies have been carried out on plasmonic heterodimers, including Au nanosphere−nanosphere with different diameters, Au nanosphere−nanoshell,[25] Au nanosphere−Ag nanosphere,[26,27] and Au nanodisk−nanodisk with different diameters.[28,29] Heterodimers composed of anisotropic Au and Ag nanorods aligned in different geometries have also been studied.[30−32] In heterodimers of metal nanocrystals, multipolar plasmon modes can be excited through near-field interactions, and the Fano interference between subradiant and superradiant plasmon modes can usually be observed. These heterodimers exhibit light responses that are dependent on the incident direction[25,28,29] and possess unique electric field distributions at different plasmon modes.[26] They therefore have potentials for nanoscale directional color router[29] and subwavelength imaging.

The plasmon coupling in metal nanocrystal heterodimers is expected to be dependent not only on the metal type and the size difference but also on the spatial arrangement of the two components. Nearly all of the plasmonic heterodimers investigated previously are rotationally symmetric about the interparticle axis, where the spatial symmetry is not completely broken. Breaking the rotational symmetry will undoubtedly provide more freedom for controlling the plasmonic properties of heterodimers. Herein, we report on the investigation of the

Received: November 22, 2011
Revised: January 17, 2012
Published: January 23, 2012

plasmon coupling in the heterodimers made of a large Au nanorod and a small Au nanosphere, where the nanosphere is located at different positions on the nanorod surface, as shown schematically in Figure 1. Au nanorods are chosen due to their

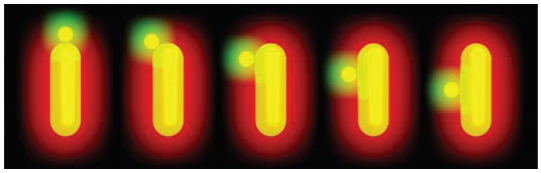

Figure 1. Schematic showing the plasmon resonance of a Au nanorod perturbed by the plasmon resonance of an adjacent small Au nanosphere that is located at different positions around the nanorod.

synthetically adjustable plasmon energies and polarization-sensitive optical responses. The anisotropic geometry of the nanorod causes the rotational symmetry to be broken as the nanosphere is moved around the nanorod. The small spatial perturbation introduced by the nanosphere generates dramatic changes in the scattering spectrum of the heterodimer. The dipole of the nanosphere rotates around that of the nanorod in the bonding dipole−dipole mode when the nanosphere is moved around the nanorod. Compared to more complex metal nanostructures supporting symmetry breaking, such as trimers and tetramers,[1,2] the Au nanorod−nanosphere heterodimers are easier to prepare, which is attractive for their practical applications. We anticipate that our results will be useful for designing plasmon rulers of two spatial coordinates and for developing plasmon-based switching devices.

The Au nanorods and nanospheres stabilized with cetyltrimethylammonium bromide (CTAB) were obtained from NanoSeedz. The Au nanorods were prepared in aqueous solutions using the standard seed-mediated growth method together with shortening.[33−35] The Au nanospheres were also made following a seeded growth method.[36] The scanning electron microscopy (SEM) image of the nanorod sample and the transmission electron microscopy (TEM) image of the nanosphere sample are shown in Figures S1a and S1b of the Supporting Information, respectively. The nanorod sample exhibits a longitudinal plasmon resonance wavelength of 654 nm in aqueous solutions and has an average length of 85 ± 6 nm, diameter of 38 ± 4 nm, and aspect ratio of 2.2 ± 0.2. The nanosphere sample has an average diameter of 24 ± 2 nm, with the plasmon resonance wavelength at 527 nm in an aqueous environment. For the formation of the heterodimers, the two nanocrystal samples were mixed and dispersed in a mixture of H_2O and CH_3CN. 1,8-Octanedithiol, as a link between the nanorods and nanospheres,[24,37] was then added in the mixture solution. The assembly process in the solution was monitored spectrally (Figure S1g). The assembled nanocrystals were deposited on conductive indium tin oxide (ITO)-coated glass slides. Figure S1c−e shows the TEM images of representative Au nanorod−nanosphere heterodimers. The position of the nanosphere relative to the nanorod varies among different heterodimers. The spacing between the two nanocrystals was estimated from high-resolution TEM images (Figure S1f) to be ∼1 nm, which is consistent with the values obtained in the previous studies.[24,37]

We utilized a pattern-matching method[24,38] to correlate the single-particle dark-field scattering spectrum (see Supporting Information for the measurement details) of each heterodimer with its geometry revealed by SEM imaging. Figure 2 shows the SEM images of four representative nanorod−nanosphere

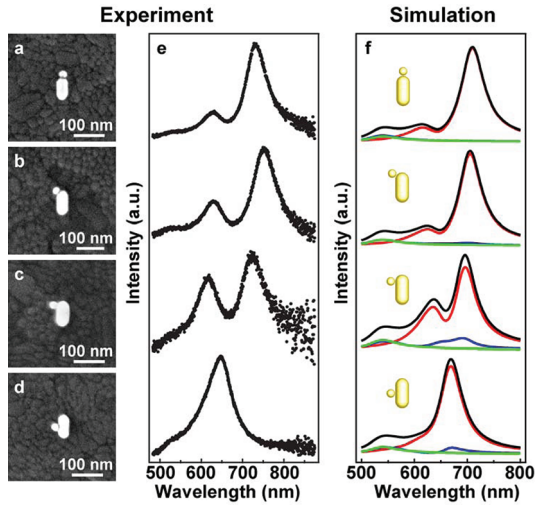

Figure 2. Plasmonic responses of four representative heterodimers. (a−d) SEM images. (e) Corresponding experimental scattering spectra. Each spectrum is normalized and shifted vertically for clarity. (f) Calculated scattering spectra. The red, blue, and green curves represent the scattering spectra when the excitation light is polarized longitudinally, transversely, and vertically, respectively. The black curves are the sums.

heterodimers with the nanosphere located at different positions on the nanorod and the corresponding scattering spectra. The scattering spectra are observed to vary systematically as a function of the position of the nanosphere on the nanorod. When the nanosphere is located at the end of the nanorod, two scattering peaks are detected, with the higher-energy one much weaker than the lower-energy one. In comparison, a single Au nanorod exhibits only one strong scattering peak.[33] The two scattering peaks of the heterodimer arise from the plasmon coupling between the nanorod and nanosphere. When the nanosphere is moved from the end through the shoulder to the side of the nanorod at a fixed gap distance, the intensity of the higher-energy peak gets relatively stronger, and the two peaks become closer spectrally. When the nanosphere is at the exact central side of the nanorod, the two scattering peaks coalesce into one. A small bump is present around 530 nm on all the scattering spectra. This weak peak is contributed mainly by the coupling between the heterodimers and the substrate and excited by light polarized perpendicular to the substrate plane.[24,38]

We measured the scattering spectra of more than 100 heterodimers. The position of the nanosphere on the nanorod is statistically randomly distributed in these heterodimers. More than 80% of the heterodimers with the nanosphere off the exact central side of the nanorod show the two peaks on their scattering spectra. The overall shapes of the scattering spectra vary systematically, as described above, although the positions and relative intensities of the two peaks also fluctuate among the heterodimers with the same geometrical arrangement under the SEM imaging resolution. The fluctuations can be ascribed to the size distributions of both the Au nanorod and nanosphere samples and the slight variation in the gap distance caused by the flexibility of the linking molecules. To exclude the conductive coupling between the nanorod and nanosphere in

dx.doi.org/10.1021/nl2041063 | Nano Lett. 2012, 12, 1424−1430

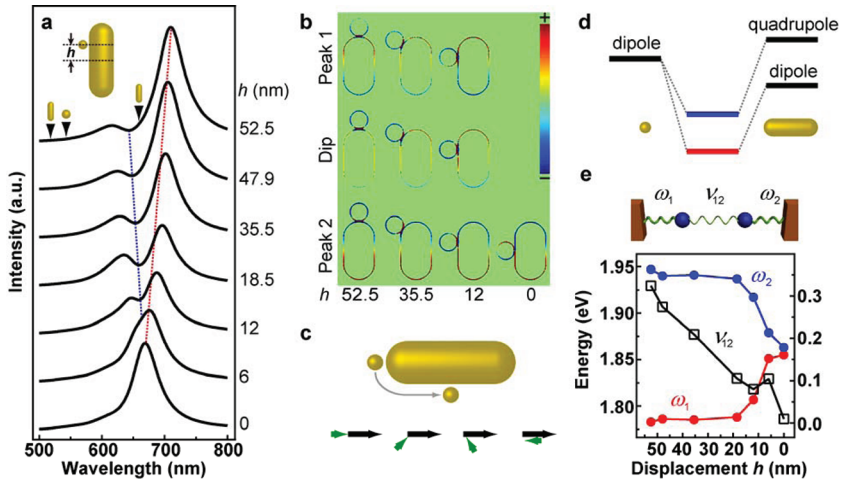

Figure 3. (a) Calculated scattering spectra of the heterodimers under the longitudinally polarized excitation. The inset shows the definition of the displacement, *h*, of the nanosphere. The spectral positions of the dipolar and quadrupolar plasmon modes of the naonrod and the dipolar plasmon mode of the nanosphere are indicated with the downward arrows. The blue and red dotted lines indicate the dip and lower-energy peak positions. (b) Charge distributions on the central cross sections of the heterodimers for the higher-energy (peak 1) and lower-energy (peak 2) scattering peaks and the dip between them. (c) Schematic elucidating how the plasmonic dipole of the nanosphere rotates around that of the nanorod as the nanosphere is moved from the end to the exact central side of the nanorod. (d) Plasmon hybridization diagram for the nanorod−nanosphere heterodimer. (e) Coupled harmonic oscillator model for the plasmonic response of the heterodimer. Oscillator 1 is driven by a periodic harmonic force. The eigenenergies of the two oscillators, ω_1 and ω_2 (red and blue, respectively, left axis), and their coupling strength, ν_{12} (black, right axis), are plotted against the displacement of the nanosphere.

the heterodimers, we performed a control experiment, where the heterodimers deposited on the ITO substrates were thermally treated. The scattering spectra of the heterodimers after the thermal treatment are dramatically different from those before the treatment (Figure S2). Such spectral changes result from the formation of conductive contacts caused by the thermal treatment.[24,38] The newly formed higher- and lower-energy peaks have been identified as the bonding and charge-transfer plasmon modes, respectively.[30] The results from this control experiment verify the existence of a gap in the nanorod−nanosphere heterodimers. Moreover, in order to reveal the origin of the different scattering peaks, we also excited the heterodimers with polarized white light.[39] The polarization measurement reveals that the two scattering peaks are excited when the white light source is polarized along the length axis of the Au nanorod (Figure S3). This finding is consistent with the previous result for the plasmon modes in Au nanosphere−nanoshell heterodimers.[25] The plasmon response excited by the light source polarized perpendicular to the length axis of the nanorod is too weak to be detected in our experiments.

Finite-difference time-domain (FDTD) calculations were carried out to understand the plasmonic properties of a nanorod perturbed by a nanosphere at varying spatial positions (see Supporting Information for the calculation details). Our previous studies have shown that ITO substrates only induce a weak scattering peak in the spectral region of 500−550 nm for relatively small Au nanostructures.[24,38−40] The simulations were therefore performed in a homogeneous medium with a refractive index of 1.45 in order to clearly unravel the involved plasmon modes. Both the nanocrystal monomers and heterodimers were considered. The Au nanorod was modeled as a cylinder capped with a hemisphere at each end. The Au nanosphere was modeled as an exact sphere. The gap distance between the nanorod and nanosphere was set at 1 nm. The nanocrystal sizes were adjusted slightly within the experimentally measured range to reach a good agreement between the calculated and measured scattering spectra. The final sizes used in the calculations were 79 nm in length and 42 nm in diameter for the nanorod and 24 nm in diameter for the nanosphere. The calculated scattering spectra of the four heterodimers with their geometrical arrangements shown in Figure 2a−d are plotted in Figure 2f for different excitation polarizations. The scattering for the excitation polarized parallel to the substrate and along the nanorod length axis (longitudinal polarization) is much stronger than that for the excitation polarized parallel to the substrate and along the direction perpendicular to the nanorod length axis (transverse polarization) and that for the excitation polarized perpendicular to the substrate (vertical polarization). The longitudinally polarized light can excite two scattering peaks, which agrees with the experimental results. A weak peak is observed around 540 nm for both the transversely and vertically polarized excitation. Taking into account of the ITO substrate will only increase the scattering intensity of this peak under the vertically polarized excitation owing to the coupling between the heterodimers and the substrate.[24,38] The overall variation trend in the calculated scattering spectra agrees qualitatively with that observed experimentally. The differences between the measured and calculated spectra are ascribed to the nanocrystal size distributions and small fluctuation in the interparticle gap distance in the experiments, the use of a homogeneous dielectric environment in the calculations, and the dissimilar excitation and collection geometries between the calculations and measurements. In particular, the higher-energy scattering peaks on the measured spectra are stronger than those on the simulated spectra. The stronger scattering peaks on the measured spectra can be attributed to smaller than 1 nm gap distances, which will be discussed below.

More simulation results are provided in Figure 3a, which illustrates how the scattering spectrum evolves as the Au nanosphere is moved from the end to the central side of the Au nanorod. A vertical displacement, *h*, was employed to designate the position of the nanosphere on the nanorod. *h* equals 0 when the nanosphere is located at the exact central side of the

dx.doi.org/10.1021/nl2041063 | *Nano Lett.* 2012, 12, 1424−1430

nanorod, and it assumes the maximal value of 52.5 nm when the nanosphere is at the end of the nanorod. Only the longitudinally polarized excitation was considered. As h is gradually decreased from 52.5 to 0 nm, the lower-energy scattering peak blue-shifts from 709 to 669 nm, while the higher-energy one first red-shifts from 616 to 647 nm and then becomes submerged under the lower-energy peak. Intriguingly, no matter where the nanosphere is placed on the nanorod, the gap region between the two nanocrystals always exhibits a large electric field enhancement at the lower-energy scattering peak, forming a so-called "hot spot" (Figure S4). This result is different from the reported reduction in the electric field in the gap region exhibited by Au nanorod dimers.[24]

To assign the hybridized plasmon modes in the heterodimers, we determined the charge distributions at different excitation wavelengths from the calculated electric field contours. The dipolar plasmon modes of the nanosphere and nanorod are at 543 nm (2.28 eV) and 659 nm (1.88 eV), respectively. The wavelength of the quadrupolar plasmon mode of the nanorod was calculated by using a dipole source[31] to be 518 nm (2.39 eV). When the nanosphere is located at the end of the nanorod, the two scattering peak wavelengths of the heterodimer were obtained to be 709 nm (1.75 eV) and 616 nm (2.01 eV). The charge distributions (Figure 3b), as well as the electric field intensity enhancement contours (Figure S5), on the central cross section of the heterodimer indicate that the two scattering peaks and the dip in between result from the hybridization of the plasmon modes of the nanorod and nanosphere. The two nanocrystals exhibit unambiguously an attractive dipole−dipole interaction at the lower-energy peak, suggesting the dominance of the bonding dipole−dipole mode at the lower-energy peak. The charge distributions of the nanosphere remain to be dipolar at both the higher-energy peak and the dip, while those of the nanorod turn out to contain both dipolar and multipolar characteristics. At the dip, the nanorod mainly exhibits a quadrupolar charge distribution. At the higher-energy peak, both dipole-dominated and quadrupole-dominated charge contours are obtained, depending on the phase angle of the excitation light wave (Figure S6). The two nanocrystals in the heterodimer, no matter what type of hybridization behaviors they present, always display an attractive manner. Therefore, the heterodimer exhibits a bonding dipole−dipole pattern at the lower-energy peak, a bonding dipole−quadrupole one at the dip, and a mixture of them at the higher-energy peak. Since the Au nanosphere in the heterodimer is much smaller than the nanorod, it exhibits only a dipolar plasmon mode. Because of the closeness in the plasmon energy levels of the monomers, the dipolar plasmon mode (2.28 eV) of the nanosphere can hybridize largely with both the dipolar (1.88 eV) and quadrupolar (2.39 eV) plasmon modes of the nanorod, forming the bonding dipole−dipole (∼1.75 eV) and dipole−quadrupole (∼1.93 eV) hybridized modes, as shown in Figure 3d.

When the nanosphere is moved away from the end of the nanorod and the displacement h is reduced, the nanosphere and nanorod both maintain their dipolar charge patterns at the lower-energy peak, which blue-shifts gradually (Figure 3a). The nanosphere rotates its plasmonic dipole as it is moved from the end to the central side of the nanorod. At the exact central side, the dipoles of the nanosphere and nanorod are oriented oppositely. Throughout the positional changes of the nanosphere on the nanorod, the two dipoles are always in attractive bonding configurations (Figure 3b,c), and the energy of the bonding dipole−dipole mode increases slightly as h is decreased. The rotating plasmonic dipole phenomenon is consistent with the hot spots observed in the electric field intensity enhancement contours (Figure S4). At the dip, the heterodimers always exhibit a bonding dipole−quadrupole mode. The slight red shift of the dip on the scattering spectra with decreasing h (Figure 3a) suggests the strengthening of the attractive interaction between the dipole of the nanosphere and the quadrupole of the nanorod.

The pronounced dips observed in both the measured and simulated scattering spectra are attributed to the Fano interference between the superradiant bonding dipole−dipole and the subradiant bonding dipole−quadrupole plasmon modes. The charge contours in Figure 3b indicate that the quadrupolar mode of the nanorod can be excited through near-field interaction in the presence of the nanosphere. It can thus hybridize with the dipolar mode of the nanosphere. Because the energies of the bonding dipole−dipole and dipole−quadrupole modes are close to each other and the former mode has a broad line width, the two modes interfere destructively at their common frequency. The destructive interference produces a Fano resonance, which is reflected by the dips on the scattering spectra.

The Fano profiles of the calculated scattering spectra of the nanorod−nanosphere heterodimers can be well reproduced by the classical two-oscillator model that has been used to describe electromagnetically induced transparency.[41,42] The bonding dipole−dipole and dipole−quadrupole plasmon modes are modeled as two interacting one-dimensional mechanical oscillators of energies ω_1 and ω_2 with an interacting strength of ν_{12} (Figure 3e). The oscillator with an energy of ω_1, corresponding to the superradiant mode, is driven by a periodic harmonic force $F(t) = F_0e^{-i\omega t}$. The equations of motion of the two oscillators are described by

$$\ddot{x}_1 + \gamma_1\dot{x}_1 + {\omega_1}^2x_1 - \nu_{12}x_2 = F_0e^{-i\omega t} \quad (1)$$

$$\ddot{x}_2 + \gamma_2\dot{x}_2 + {\omega_2}^2x_2 - \nu_{12}x_1 = 0 \quad (2)$$

where x_i specifies the displacement from the equilibrium position of the oscillator and γ_i represents the friction coefficient accounting for the energy dissipation of the oscillator. The equations can be solved in the form $x_i = c_ie^{-i\omega t}$. The scattering power of the system is expressed by $P(\omega) = |\ddot{x}_1 + \ddot{x}_2|^2$. The scattering spectra calculated from the two-oscillator model fit the FDTD simulation results very well (Figure S7). Figure 3e shows the variations of ω_1, ω_2, and ν_{12} as a function of h. The variation trends of ω_1 and ω_2 agree well with the FDTD simulation results. As the nanosphere is moved away from the end of the nanorod, the dipole−dipole bonding energy ω_1 increases and the dipole−quadrupole bonding energy ω_2 decreases. We also find that ω_1 and ω_2 change rapidly after the nanosphere enters into the cylindrical body region of the nanorod, where h is less than 18.5 nm. In addition, the interaction strength between the two bonding plasmon modes ν_{12} generally becomes weaker with decreasing h. The reduction in the interaction strength can be attributed to the decrease in the oscillator strengths of the two bonding modes. The Fano dip disappears when the nanosphere arrives at the exact central side of the nanorod, where h equals 0. Despite nearly the same energy of the two bonding plasmon modes at this position, the quadrupolar mode of the nanorod can hardly be excited, owing to the increase in the symmetry of

dx.doi.org/10.1021/nl2041063 | Nano Lett. 2012, 12, 1424−1430

the system. As a result, the oscillator strength of the bonding dipole−dipole mode is much larger than that of the dipole−quadrupole mode, and the interaction strength ν_{12} becomes very small.

The evolving mechanism of the scattering spectrum as a function of the position of the nanosphere on the nanorod has been understood above. We next studied the effects of the gap distance and the nanocrystal dimensions on the plasmonic response of the nanorod perturbed by the nanosphere by placing the nanosphere at the end of the nanorod. Figure 4a shows how the scattering spectrum of the nanorod−nanosphere heterodimer changes as the gap distance d is varied. At a very small d value of 0.5 nm, the heterodimer displays a distinct Fano profile on its scattering spectrum. As d is increased, the higher-energy scattering peak gets weaker while the lower-energy peak becomes stronger, indicating the gradual weakening of the destructive Fano interference between the bonding dipole−dipole and dipole−quadrupole plasmon modes. The double-peak spectral feature vanishes when d is larger than 1.5 nm. The gap distance-dependent result indicates that the perturbation caused by the nanosphere is remarkably sensitive to the gap distance. We then fixed the gap distance at 1 nm and changed the nanorod length L. The lower-energy peak increases in intensity and exhibits a gradual red shift with increasing L, while the higher-energy peak decreases slightly in intensity and red-shifts slightly (Figure 4b). The red shift of the bonding dipole−dipole mode is mainly caused by the red shift of the longitudinal dipolar mode of the nanorod as its aspect ratio is increased. The intensity increase of the lower-energy peak results from the increase in the polarizability of the nanorod as L gets larger. We further fixed the gap distance d at 1 nm and the nanorod length L at 79 nm and varied the nanosphere diameter D. The gradual enlargement of the nanosphere leads to the red shift of its dipolar plasmon mode and consequently the red shift of the bonding dipole−dipole mode of the heterodimer, but the higher-energy scattering peak wavelength remains nearly unchanged (Figure 4c). Both the lower- and higher-energy scattering peaks increase slightly in intensity with D due to the increase in the polarizability of the nanosphere. Moreover, we examined the effect of the gap distance on the scattering spectra of the heterodimers with the

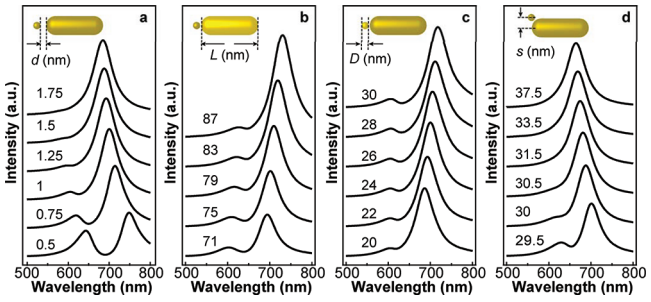

Figure 4. Calculated scattering spectra of the Au nanorod−nanosphere heterodimers. (a) The nanosphere is at the end of the nanorod. The gap distance d is varied. (b) The nanosphere is at the end of the nanorod with a gap distance of 1 nm. The nanorod length L is varied. (c) The nanosphere is at the end of the nanorod with a gap distance of 1 nm. The nanosphere diameter D is varied. (d) The vertical displacement h is fixed at 35.5 nm. The lateral displacement s is varied. The excitation light is longitudinally polarized. The insets show the schematics of the heterodimers.

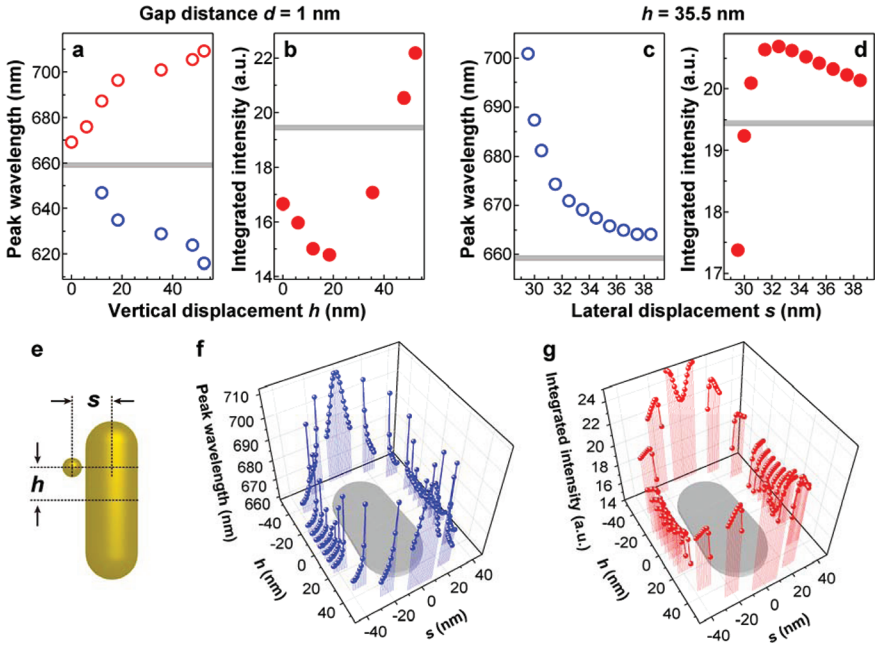

Figure 5. (a) Wavelengths of the two scattering peaks as a function of the vertical displacement h when the gap distance d between the nanorod and nanosphere is fixed at 1 nm. The data were extracted from the calculated scattering spectra shown in Figure 3a. The red and blue colors denote the data points for the lower- and higher-energy peaks, respectively. (b) Integrated scattering intensity of the heterodimer versus h when d is fixed at 1 nm. (c) Wavelength of the lower-energy scattering peak as a function of the lateral displacement s when h is fixed at 35.5 nm. The data were extracted from the calculated scattering spectra shown in Figure 4d. (d) Integrated scattering intensity of the heterodimer versus s when h is fixed at 35.5 nm. The gray bars in (a−d) represent the corresponding values of a single Au nanorod. (e) Schematic of the coordinate system. (f) Wavelength of the lower-energy scattering peak as a function of both h and s. (g) Integrated scattering intensity as a function of both h and s. The gray elliptical shadows in (f) and (g) indicate the positions of the nanorods. The excitation light is longitudinally polarized.

dx.doi.org/10.1021/nl2041063 | Nano Lett. 2012, 12, 1424−1430

nanosphere placed at different vertical displacements. The lateral displacement s of the nanosphere, defined by the distance from the nanosphere center to the nanorod length axis, was increased gradually to enlarge the gap distance d. As an example, Figure 4d shows how the scattering spectrum of the heterodimer changes as s is varied while the vertical displacement h is fixed at 35.5 nm. Similar to the case shown in Figure 4a, the heterodimer only displays a distinct Fano profile on its scattering spectrum at small gap distances. As s is increased, the lower-energy scattering peak blue-shifts gradually. The double-peak spectral feature vanishes when s reaches 30.5 nm, which corresponds to a gap distance of d = 1.9 nm. The spatial perturbation of the nanosphere on the plasmonic response of the nanorod is thereafter found to be extraordinarily sensitive to the gap distance and affected by the nanorod dimension. It is less sensitive to the size of the nanosphere. These results further explain the origins of the differences between our measured and calculated scattering spectra. In the experiments, the plasmonic features reflected on the scattering spectra are affected by the fluctuations in the gap distance and the nanocrystal sizes.

We finally extracted the scattering peak wavelengths and intensities from the calculated scattering spectra and plotted them versus the positions of the perturbing nanosphere in Figure 5. As described above, when the gap distance d is fixed at 1 nm, the wavelength of the lower-energy scattering peak becomes shorter and that of the higher-energy one gets longer with decreasing vertical displacement h (Figure 5a). The intensity of the lower-energy peak first decreases as the nanosphere is moved away from the end of the nanorod and then increases after the nanosphere enters into the cylindrical body region of the nanorod. The intensity of the higher-energy peak, in contrast, exhibits a monotonic increase (Figure S8). We also integrated the scattering intensity, which is an easy-to-measure quantity, from 500 to 800 nm and plotted it as a function of the vertical displacement h of the nanosphere in Figure 5b. The integrated intensity exhibits first a decrease and then an increase as the nanosphere is moved away from the end of the nanorod. The turning point also occurs when the nanosphere enters into the cylindrical body of the nanorod. On the other hand, when h is fixed at 35.5 nm, the wavelength of the lower-energy scattering peak becomes shorter and thereafter closer to the longitudinal plasmon wavelength of the nanorod as the lateral displacement s is increased (Figure 5c). The integrated intensity first rises rapidly and then falls down slowly as s is increased from 29.5 to 38.5 nm (Figure 5d). The rapid intensity increase results from the fast weakening of the destructive Fano interference between the two bonding plasmon modes as the gap distance is increased. The subsequent decrease of the intensity originates from the reduction of the plasmon coupling strength between the two nanocrystals. The wavelength of the lower-energy scattering peak and the integrated scattering intensity of the heterodimer are further plotted as functions of both the vertical displacement h and the lateral displacement s (Figure 5e–g). The continuous blue shift of the peak wavelength indicates the weakening of the plasmon coupling as the nanosphere is moved away from the nanorod. The scattering intensity generally exhibits a rapid decrease when the nanosphere gets very close to the nanorod. These dependences allow for the determination of the spatial position of the perturbing nanosphere relative to the nanorod by monitoring the scattering peak wavelength and the total scattering intensity. The Au nanorod–nanosphere heterodimers therefore offer a potential means for measuring nanometric distance changes that are involved in biological and nanoelectromechanical systems.

In summary, we have shown that the spatial perturbation of a Au nanosphere attached to a Au nanorod induces distinct variations on the scattering spectrum of the heterodimer. The plasmon resonance of the Au nanorod is strongly modulated by that of the small nanosphere. As the nanosphere is moved around the nanorod, the rotational symmetry of the Au nanorod–nanosphere heterodimer is broken, causing the coupled plasmon modes and their Fano interference to vary. The dipole of the nanosphere rotates around that of the nanorod and maintains favorable attractive configurations for the bonding dipole–dipole mode. The gap region between the two nanocrystals therefore always exhibits an electric field "hot spot". In addition, the plasmonic responses of the heterodimers are found to be highly sensitive to the gap distance and affected by the sizes of the constituting monomers. The breaking of the rotational symmetry provides an additional freedom for controlling the plasmonic properties of metal nanocrystal heterodimers. The optical response of the heterodimer system varies with both the vertical and lateral displacements of the nanosphere. In particular, it is extremely sensitive to the movement of the nanosphere when the gap distance between the two nanocrystals is less than ~2 nm. We therefore expect that the nanorod–nanosphere system will offer a useful means for measuring the transformations of macromolecules in soft-matter systems. Molecules can be conjugated to small Au nanospheres. Molecular transformations can then be detected in real time by monitoring the plasmon coupling between the nanospheres and Au nanorods deposited or lithographically fabricated on substrates. A lookup database will be needed for determining the positions of the nanospheres relative to the nanorods accurately. As a result, the distinct plasmonic manifestations on Au nanorods induced by the spatial perturbations of Au nanospheres enable the use of dark-field scattering spectroscopy to identify the spatial movements of a metal nanocrystal at nanometric precision. The Au nanorod–nanosphere heterodimers can therefore be utilized as a potential plasmon ruler of two spatial coordinates.

■ ASSOCIATED CONTENT

Supporting Information

Instrumentation and FDTD calculation details, the SEM and TEM images of the Au nanosphere, nanorod, and heterodimer samples, the extinction spectra of the assembly process, the scattering spectra of the heterodimers before and after the thermal treatment, the scattering spectra of the heterodimers under polarized excitation, the field intensity enhancement contours for the nanosphere placed at different positions on the nanorod, the field intensity enhancement contours at the two scattering peaks and the dip for the nanosphere placed at the end of the nanorod, the charge contours of a heterodimer at the higher-energy scattering peak, the intensity of the scattering peaks versus the vertical displacement, and the calculated scattering spectra fitted with the two-harmonic oscillator model. This material is available free of charge via the Internet at http://pubs.acs.org.

■ AUTHOR INFORMATION

Corresponding Author

*E-mail: jfwang@phy.cuhk.edu.hk.

Author Contributions

[§]These authors contributed equally to this work.

Notes

The authors declare no competing financial interest.

■ ACKNOWLEDGMENTS

This work was supported by Hong Kong RGC GRF grant (ref. no.: CUHK403409; Project Code: 2160391), RGC Direct Allocation (Project Code: 2060417), and MOST of China (grant no.: 2011CB922200). The FDTD simulations in this work were conducted in the High Performance Cluster Computing Centre, Hong Kong Baptist University, which is supported by Hong Kong RGC and Hong Kong Baptist University.

■ REFERENCES

(1) Halas, N. J.; Lal, S.; Chang, W.-S.; Link, S.; Nordlander, P. *Chem. Rev.* **2011**, *111*, 3913−3961.
(2) Fan, J. A.; Wu, C.; Bao, K.; Bao, J. M.; Bardhan, R.; Halas, N. J.; Manoharan, V. N.; Nordlander, P.; Shvets, G.; Capasso, F. *Science* **2010**, *328*, 1135−1138.
(3) Liu, N.; Guo, H. C.; Fu, L. W.; Kaiser, S.; Schweizer, H.; Giessen, H. *Nat. Mater.* **2008**, *7*, 31−37.
(4) Luk'yanchuk, B.; Zheludev, N. I.; Maier, S. A.; Halas, N. J.; Nordlander, P.; Giessen, H.; Chong, C. T. *Nat. Mater.* **2010**, *9*, 707−715.
(5) Liu, N.; Langguth, L.; Weiss, T.; Kästel, J.; Fleischhauer, M.; Pfau, T.; Giessen, H. *Nat. Mater.* **2009**, *8*, 758−762.
(6) Prodan, E.; Radloff, C.; Halas, N. J.; Nordlander, P. *Science* **2003**, *302*, 419−422.
(7) Merlein, J.; Kahl, M.; Zuschlag, A.; Sell, A.; Halm, A.; Boneberg, J.; Leiderer, P.; Leitenstorfer, A.; Bratschitsch, R. *Nat. Photonics* **2008**, *2*, 230−233.
(8) Huang, F. M.; Baumberg, J. J. *Nano Lett.* **2010**, *10*, 1787−1792.
(9) Sun, Z. H.; Ni, W. H.; Yang, Z.; Kou, X. S.; Li, L.; Wang, J. F. *Small* **2008**, *4*, 1287−1292.
(10) Sönnichsen, C.; Reinhard, B. M.; Liphardt, J.; Alivisatos, A. P. *Nat. Biotechnol.* **2005**, *23*, 741−745.
(11) Liu, N.; Hentschel, M.; Weiss, T.; Alivisatos, A. P.; Giessen, H. *Science* **2011**, *332*, 1407−1410.
(12) Rosi, N. L.; Mirkin, C. A. *Chem. Rev.* **2005**, *105*, 1547−1562.
(13) Liu, N.; Weiss, T.; Mesch, M.; Langguth, L.; Eigenthaler, U.; Hirscher, M.; Sönnichsen, C.; Giessen, H. *Nano Lett.* **2010**, *10*, 1103−1107.
(14) Verellen, N.; Van Dorpe, P.; Huang, C. J.; Lodewijks, K.; Vandenbosch, G. A. E.; Lagae, L.; Moshchalkov, V. V. *Nano Lett.* **2011**, *11*, 391−397.
(15) Large, N.; Abb, M.; Aizpurua, J.; Muskens, O. L. *Nano Lett.* **2010**, *10*, 1741−1746.
(16) Ueno, K.; Juodkazis, S.; Shibuya, T.; Yokota, Y.; Mizeikis, V.; Sasaki, K.; Misawa, H. *J. Am. Chem. Soc.* **2008**, *130*, 6928−6929.
(17) Kim, S.; Jin, J.; Kim, Y.-J.; Park, I.-Y.; Kim, Y.; Kim, S.-W. *Nature* **2008**, *453*, 757−760.
(18) Grigorenko, A. N.; Roberts, N. W.; Dickinson, M. R.; Zhang, Y. *Nat. Photonics* **2008**, *2*, 365−370.
(19) Lim, D.-K.; Jeon, K.-S.; Kim, H. M.; Nam, J.-M.; Suh, Y. D. *Nat. Mater.* **2010**, *9*, 60−67.
(20) Schietinger, S.; Aichele, T.; Wang, H.-Q.; Nann, T.; Benson, O. *Nano Lett.* **2010**, *10*, 134−138.
(21) Kinkhabwala, A.; Yu, Z. F.; Fan, S. H.; Avlasevich, Y.; Müllen, K.; Moerner, W. E. *Nat. Photonics* **2009**, *3*, 654−657.
(22) Nordlander, P.; Oubre, C.; Prodan, E.; Li, K.; Stockman, M. I. *Nano Lett.* **2004**, *4*, 899−903.
(23) Jain, P. K.; Eustis, S.; El-Sayed, M. A. *J. Phys. Chem. B* **2006**, *110*, 18243−18253.
(24) Shao, L.; Woo, K. C.; Chen, H. J.; Jin, Z.; Wang, J. F.; Lin, H.-Q. *ACS Nano* **2010**, *4*, 3053−3062.
(25) Brown, L. V.; Sobhani, H.; Lassiter, J. B.; Nordlander, P.; Halas, N. J. *ACS Nano* **2010**, *4*, 819−832.
(26) Sheikholeslami, S.; Jun, Y.-W.; Jain, P. K.; Alivisatos, A. P. *Nano Lett.* **2010**, *10*, 2655−2660.
(27) Bachelier, G.; Russier-Antoine, I.; Benichou, E.; Jonin, C.; Del Fatti, N.; Vallée, F.; Brevet, P.-F. *Phys. Rev. Lett.* **2008**, *101*, 197401.
(28) Pakizeh, T.; Käll, M. *Nano Lett.* **2009**, *9*, 2343−2349.
(29) Shegai, T.; Chen, S.; Miljković, V. D.; Zengin, G.; Johansson, P.; Käll, M. *Nat. Commun.* **2011**, *2*, 481.
(30) Slaughter, L. S.; Wu, Y. P.; Willingham, B. A.; Nordlander, P.; Link, S. *ACS Nano* **2010**, *4*, 4657−4666.
(31) Woo, K. C.; Shao, L.; Chen, H. J.; Liang, Y.; Wang, J. F.; Lin, H.-Q. *ACS Nano* **2011**, *5*, 5976−5986.
(32) Yang, Z.-J.; Zhang, Z.-S.; Zhang, W.; Hao, Z.-H.; Wang, Q.-Q. *Appl. Phys. Lett.* **2010**, *96*, 131113.
(33) Ni, W. H.; Kou, X. S.; Yang, Z.; Wang, J. F. *ACS Nano* **2008**, *2*, 677−686.
(34) Tsung, C.-K.; Kou, X. S.; Shi, Q. H.; Zhang, J. P.; Yeung, M. H.; Wang, J. F.; Stucky, G. D. *J. Am. Chem. Soc.* **2006**, *128*, 5352−5353.
(35) Ming, T.; Kou, X. S.; Chen, H. J.; Wang, T.; Tam, H.-L.; Cheah, K.-W.; Chen, J.-Y.; Wang, J. F. *Angew. Chem., Int. Ed.* **2008**, *47*, 9685−9690.
(36) Jana, N. R.; Gearheart, L.; Murphy, C. J. *Langmuir* **2001**, *17*, 6782−6786.
(37) Pramod, P.; Thomas, K. G. *Adv. Mater.* **2008**, *20*, 4300−4305.
(38) Chen, H. J.; Sun, Z. H.; Ni, W. H.; Woo, K. C.; Lin, H.-Q.; Sun, L. D.; Yan, C. H.; Wang, J. F. *Small* **2009**, *5*, 2111−2119.
(39) Chen, H. J.; Shao, L.; Ming, T.; Woo, K. C.; Man, Y. C.; Wang, J. F.; Lin, H.-Q. *ACS Nano* **2011**, *5*, 6754−6763.
(40) Chen, H. J.; Ming, T.; Zhang, S. R.; Jin, Z.; Yang, B. C.; Wang, J. F. *ACS Nano* **2011**, *5*, 4865−4877.
(41) Alzar, C. L. G.; Martinez, M. A. G.; Nussenzveig, P. *Am. J. Phys.* **2002**, *70*, 37−41.
(42) Mukherjee, S.; Sobhani, H.; Lassiter, J. B.; Bardhan, R.; Nordlander, P.; Halas, N. J. *Nano Lett.* **2010**, *10*, 2694−2701.